Atomic-scale structure of a $SrTiO_3$ bicrystal boundary studied by scanning tunneling microscopy

Q. D. Jiang
Max-Planck-Institut für Festkörperforschung, Heisenbergstrasse 1, D-70569 Stuttgart, Germany and TcSUH, The University of Houston, Houston, Texas 77204

X. Q. Pan
Department of Materials and Engineering, University of Michigan, Ann Arbor, Michigan 48109

J. Zegenhagen
Max-Planck-Institut für Festkörperforschung, Heisenbergstrasse 1, D-70569 Stuttgart, Germany
(Received 17 April 1997)

An atomically flat and well ordered $c(6\times2)(001)$ surface of a [100] tilted ($2\times12°$) artificial $SrTiO_3$ bicrystal was prepared by thermal annealing in oxygen and ultrahigh vacuum, and characterized with low-energy electron diffraction and scanning tunneling microscopy. The real-space images of the boundary show that the bicrystal boundary is not straight, but zigzagged along the [100] and [010] crystal axis, and grooved with a depth of several atomic steps down to the bulk. We attribute the observed boundary structure to strong thermal etching and crystal faceting effects. A simple model is proposed for the path of superconducting currents of high-T_c thin films crossing such a bicrystal boundary. The model yields a $1/\tan(\theta)$ dependence of the critical current crossing the bicrystal boundary, which explains very well the reported experimental data. [S0163-1829(97)09935-9]

The discovery of the Josephson weak-link behavior of the superconducting current across grain boundaries of high-T_c cuprates[1] has led to considerable research effort into the fabrication and characterization of devices based on artificial bicrystal grain boundary (BGB) Josephson junctions.[2–6] Dinos *et al.* reported that the critical current density of YBCO films deposited on various tilted bicrystal substrates showed approximately a $1/\theta$ dependence, where θ is the angle between the [100] axes of the two crystals. Due to the very short superconducting coherence length of high-T_c cuprates, grain boundary Josephson junctions of these materials exhibit some advantages, such as high reproducibility and easily controllable processing of devices. Moreover, various experiments based on artificial grain boundary (GB) junctions[7–9] have been used to investigate the symmetry of the superconducting order parameter in high-T_c cuprates. A knowledge of the bicrystal boundary structure of the substrates is thus important for a better control of junction processing and a further understanding of the intrinsic characteristics of the grain-boundary junctions.

High-resolution TEM (Ref. 10) and x-ray diffraction[11] have revealed a very sharp interface (about 8–12 Å) at buried $\Sigma=5$ $SrTiO_3$ bicrystal boundaries. Using TEM, both c-axis-oriented $YBa_2Cu_3O_{7-\delta}$ thin films and $SrTiO_3$ bicrystal substrates (36.8°, 53.2°, and 67°) were examined in cross-sectional and in-plane views by Traeholt *et al.*[12] They observed several features of the $SrTiO_3$ and YBCO grain boundaries. Plane-view TEM showed an almost straight BGB of the $SrTiO_3$ substrate. Only some randomly located faceted voids and grooves were observed. However, the GB of the YBCO overlayer was not straight, but zigzagged. Even the position of the YBCO boundary deviated significantly from the underlying boundary of the substrate. Although TEM experiments provide valuable information about the structure of BGBs, the use of this technique requires the destruction of the sample. In this paper, we report the application of scanning tunneling microscopy to the investigation of the microscopic structure of a $SrTiO_3$ bicrystal boundary. This nondestructive technique provides information directly on the surface morphology and boundary structure of the bicrystal prior to the deposition of the T_c thin film. High-resolution transmission electron microscopy (HRTEM) was employed to provide complementary insight about the bicrystal boundary structures.

A commercially available $2\times12°$ [100] tilted $SrTiO_3$ bicrystal with a common (001) surface of the two single-crystal constituents was used in this study. A $10\times10\times0.5$-mm^3 substrate was cut into three pieces for scanning tunneling microscopy (STM) and HRTEM observations, which we conducted with a JEOL JEM-4000EX electron microscope operating at 400 kV. We performed HRTEM on both an as-received bicrystal and a two-step annealed (see below) bicrystal, whose surface was studied with STM.

Figure 1 (top) schematically shows the $SrTiO_3$ crystal structure and the geometry of the bicrystal. By Laue x-ray-diffraction patterns, the tilting angles were found to be not symmetric, with $\theta_A=10.5\pm0.5°$ and $\theta_B=13.5\pm0.5°$. The surface was cleaned with organic solvents and deionized water and subsequently annealed in O_2 at 1100 °C for 4 h. Afterwards it was loaded into the ultrahigh-vacuum (UHV) system (base pressure 5×10^{-11} mbar) for further annealing at about 950 °C for 1 h, and then cooled down to room temperature. The pressure during UHV annealing rose up to 3×10^{-8} mbar (mostly due to an increase of the oxygen partial pressure). Annealing a substrate in oxygen at high temperature is a usual procedure to remove mechanical dam-

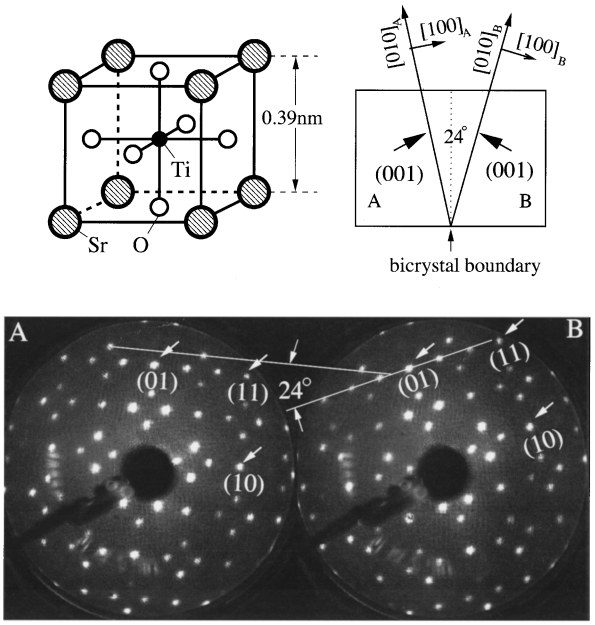

FIG. 1. Top: Schematic diagram of $SrTiO_3$ crystal structure and geometry of a bicrystal used in this study; Bottom: LEED patterns (32.4 eV) taken on *A* and *B* parts of bicrystal (001) surfaces showing a well-ordered $c(6\times2)$ reconstruction.

age due to surface polishing. Such annealing also improves the surface flatness. The second step, annealing in UHV, generates oxygen vacancies in insulating $SrTiO_3$, producing enough conductivity for scanning tunneling microscopy. The annealed surface was examined with low-energy electron diffraction (LEED), Auger-electron spectroscopy, and STM.

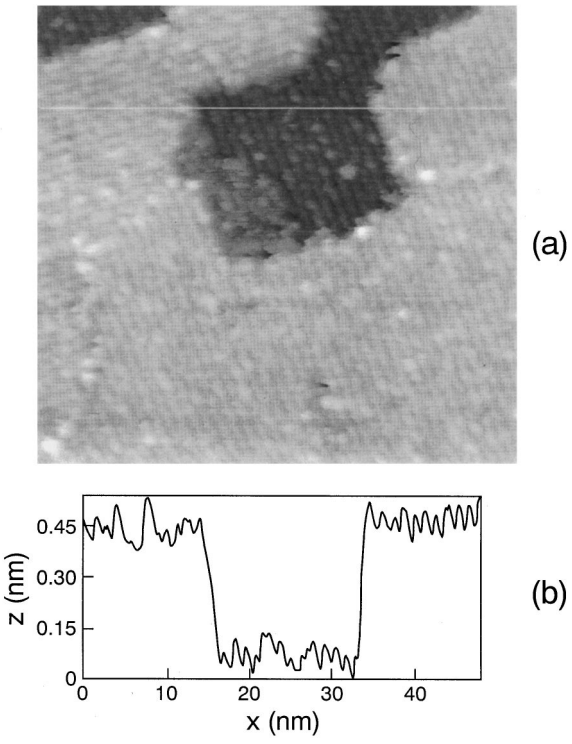

FIG. 2. STM constant current topograph (50×50 nm^2, $V_{\text{bias}}=1.9$ V, $I_T=0.23$ nA) of the $c(6\times2)$ exhibiting 90° row structures and surface steps.

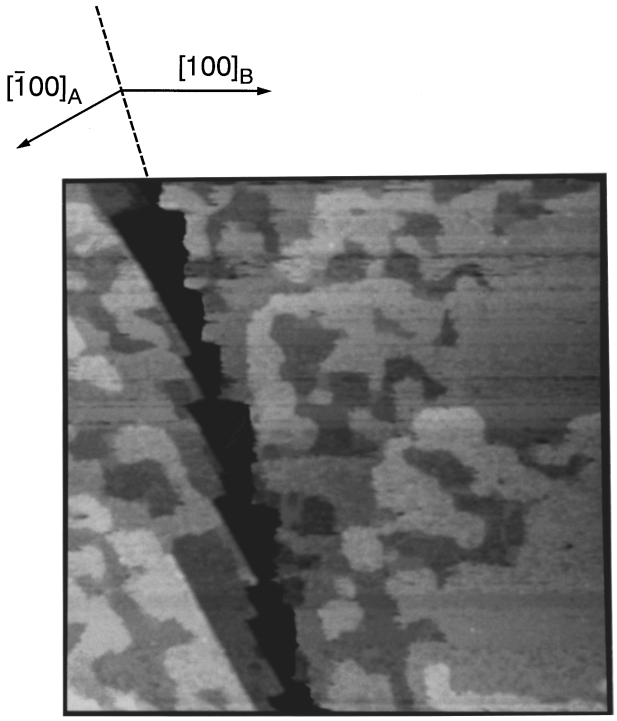

FIG. 3. STM constant current topograph (350×350 nm^2, $V_{\text{bias}}=2.0$ V, $I_T=0.4$ nA) of the $SrTiO_3$ bicrystal boundary after annealing at high temperature first in oxygen and later in UHV.

Annealing $SrTiO_3$(001) in oxygen results in a centered 6×2 reconstruction.[13,14] We recently found that our two-step annealing procedure generates a remarkably well-ordered, $c(6\times2)$ surface which is also extremely stable.[15] Such ordered $c(6\times2)$ extends over the entire surface and can be atomically resolved with STM. These properties of the $c(6\times2)$ reconstruction render it possible to locate the atomically sharp bicrystal boundary easily with STM. Moreover, the well ordered and atomically flat $SrTiO_3(001)$-$c(6\times2)$ allows stable imaging with STM, and permits one to resolve clearly details of the morphology and the atomic structure of such a $SrTiO_3$ artificial BGB.

The LEED patterns of parts *A* and *B* of the bicrystal surface are shown at the bottom of Fig. 1. The angle between the [100] axes of the crystal parts *A* and *B* is indicated. The individual LEED patterns of parts *A* and *B* are characteristic of the $c(6\times2)$ reconstruction of the $SrTiO_3$ (001) surface, covering each, the surfaces of parts *A* and *B*, with two domains, rotated by 90°, as can be seen from the outlined (reciprocal space) unit cells. Figure 2 displays a real-space STM constant current topograph of a $c(6\times2)$ surface exhibiting a row structure. The distance between the rows is 1.2 nm, three times the bulk lattice constant of $SrTiO_3$. Domains, rotated by 90° with respect to each other and single atomic steps (0.39 nm) can be seen clearly. The $SrTiO_3$-$c(6\times2)$ reconstruction was described in detail in another publication.[15]

Figure 3 shows a large-scale STM image of the bicrystal boundary in a planar view. Apparently, the surfaces on both parts of the crystal are atomically flat. Terraces are well ordered with the $c(6\times2)$ reconstruction and exhibit steps with single unit-cell height. The bicrystal boundary appears as an almost regular chain of triangular grooves. The edges

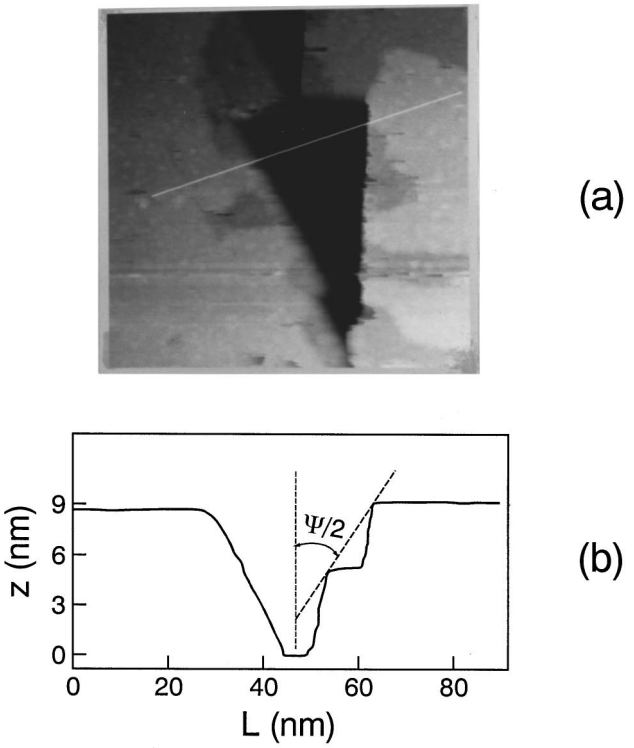

FIG. 4. (a) Close view of the faceted and grooved boundary and (b) a line profile showing steps. The image ($100\times100\ nm^2$) was scanned from left to right and taken with $V_{bias}=2.0$ V, $I_T=0.4$ nA. (c) High-resolution STM image ($V_{bias}=1.9$ V, $I_T=0.36$ nA) shows an ordered reconstruction at the bottom of the grooves.

of the grooves are aligned predominantly along the ⟨10⟩ (we use a two-dimensional notation for convenience) axis of the crystal parts *A* and *B*, resulting in zigzagging, instead of a straight line at the surface of the BGB. The width (referred to as the gap in the following discussion) of the grooves is about 20 nm at its maximum. The depth of the holes within the gap depends on the detailed structure of the boundary. It can be as deep as about 9 nm, as shown in Fig. 4, a close view (a) and a cross-section profile (b) of the BGB. A well-ordered $c(6\times2)$ reconstruction was occasionally observed at the bottom of some grooves [Fig. 4(c)]. The row direction in Fig. 4(c) corresponds to the $c(6\times2)$ structure, extending from part *A* of the crystal. This result indicates that the BGB in the bulk may also not be straight. The two crystal parts, sharing a common (001) plane, may be interlocked. From our observations, a zigzagging boundary structure from the surface down to the bulk may occur.

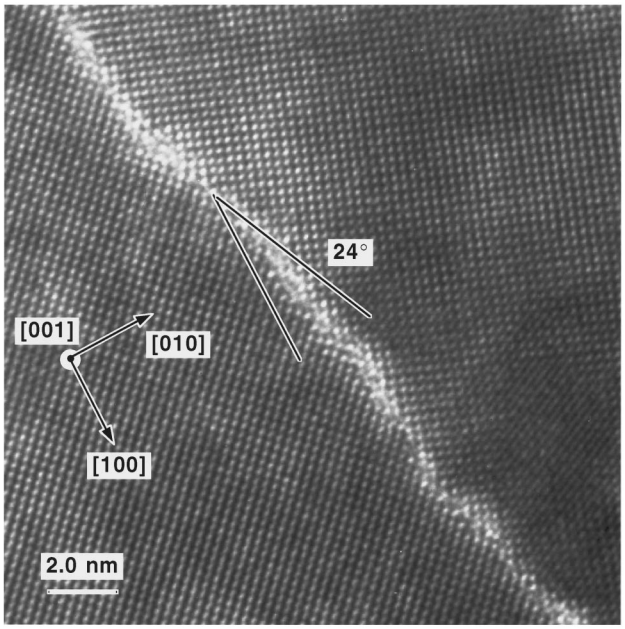

FIG. 5. HRTEM image of an as-received bicrystal displaying zigzagging of the BGB. The image contrast shows triangular shaped disordered structures at the BGB.

Figure 5 shows a HRTEM micrograph taken under a defocusing of about 60 nm from the same as-received bicrystal as that studied with STM. Computer image simulation of $SrTiO_3$thin specimens (1–20 nm) suggested that the bright spots in Fig. 5 correspond to the projection of Sr and Ti columns along [001]. Although an interpretation of TEM pictures in terms of the atomic structure of the boundary requires detailed computer image simulations and quantitative image processing, some information can be extracted by looking at the micrograph in Fig. 5. The HRTEM micrograph suggests that the BGB is very sharp, with disordered structures less than $4a_{STO}$ in width. The BGB zigzags, in agreement with the STM observations described above. The image contrast near the boundary is enhanced approaching the boundary core. The reason for this may be due to specimen thickness variations resulting from the preferential thinning at the boundary by ion milling, since the atomic binding at the boundary should be weaker than in the bulk. This means that on the surface there will be grooves along the boundary. Looking carefully at the image contrast in the TEM picture along the boundary, one can see that the grooves exhibit a triangular shape, similar to the grooves appearing in the STM image of Fig. 3, except for the size which appears to be larger in the STM image. As discussed below, the high-temperature thermal annealing of the surface in UHV can lead to the formation of large grooves.

It has been reported that only highly symmetric grain boundaries (such as $\Sigma5$) are stable and clean.[16] For grain boundaries with lower symmetry, amorphous phases and chemical precipitation appear.[16] Due to weaker atomic binding at the boundary interface, preferential thermal etching first removes disordered atoms at the boundary core. We observed that (001) $SrTiO_3$ surfaces and some vicinal (001) surfaces[17] are very stable upon high-temperature annealing. However, a vicinal (001) surface with a miscut of only about

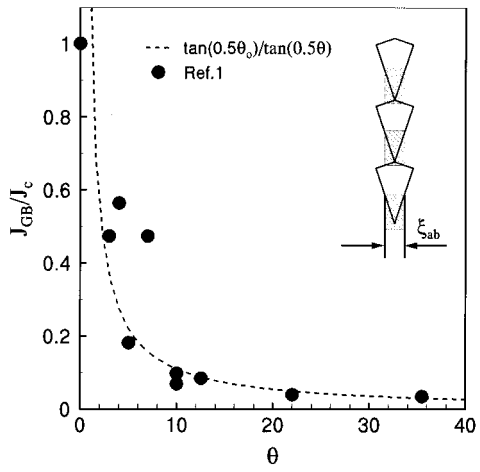

FIG. 6. Comparison of the critical current density crossing bicrystal boundaries based on the model calculation (dashed line) with experimental data (dots, From Dinos *et al.*, Ref. 1) as a function of tilting angle. Inset: A simple model of the supercurrent in a high-T_c thin film flowing across a BGB. The shaded area indicates the effective supercurrent path at the BGB.

1.2° off the (001) plane can give rise to step instability which can generate multiple unit-cell size surface steps [with (001) terraces] after a two-step thermal annealing.[15] The bicrystal boundary studied in this work is very close to a (105) interface, which appears to be unstable. After removing disordered atoms at the boundary core during annealing, step instabilities may be responsible for further removal of atoms from the boundary, leading to large grooves at the surface near the bicrystal boundary.

Considering further the requirement for the thermodynamic equilibrium, i.e., minimization of the free energy, at the solid/solid and solid/vapor interfaces at the bicrystal boundary surface, the grooving angle ψ is determined by[18]

$$\gamma_{ss} = 2\gamma_{sv}\cos(0.5\psi),$$

where γ_{ss} and γ_{sv} are the solid/solid and solid/vapor interfacial energies, respectively. From the line profile in Fig. 4, the ratio of the interfacial energy γ_{ss}/γ_{sv} can be roughly estimated to be about 1.7 for a $SrTiO_3$ grain boundary close to the (001) surface.

Using such a bicrystal as a substrate for high- T_c thin-film deposition, the morphology of the underlying substrate surfaces at the bicrystal boundary will affect the growth of the overlayer. This can explain the above-mentioned finding that the boundary of the epitaxial overlayer deviates largely from that of the underlying bicrystal even at the early stage of the growth.[12] Upon nucleation, the thin film will first start to grow on three equivalent {100} facets, which will result in the growth of grains with different orientations. As the film grows thicker, the mixed orientations will meet and develop an ill-defined structure. Degradation of the thin-film quality at the bicrystal boundary thus occurs, and may be accompanied by precipitation of impurity or even amorphous phases.

If we now consider that a grain-boundary Josephson junction is fabricated with a thin film deposited on such a bicrystal substrate, the zigzagging and grooved bicrystal boundary will consequently affect the path of the superconducting current across it on a microscopic scale. A macroscopic junction will consist of some hundreds of microjunctions. Assuming that the size of the triangular grooves (i.e., the gap) increases with increasing tilting angle of the bicrystals, the number of effective paths for the supercurrent will also decrease, thus limiting the overall critical current. This is qualitatively in agreement with the finding that the critical current density decreases with increasing tilting angle.

For simplicity, we model the current across such a boundary by taking the case of a symmetric bicrystal, and assume that all triangles have the same size and tilting angles equal to 0.5θ, as schematically shown in the inset of Fig. 6. Such morphology is expected to extend through the deposited high-T_c thin films, and will lead to degraded superconducting properties at the boundary region. Along the bicrystal boundary, there will be a nonuniform distribution of local critical currents flowing across the boundary. We can further simplify the problem by assuming that, by means of the proximity effect, the supercurrents can only cross the boundary in areas (shaded in Fig. 6), where the width of the degraded region is less than the superconducting coherence length ξ. The width w of the gap is in our case about 20 nm, and thus much larger than the superconducting coherence length ξ, which is about 1.5 nm for YBCO in the ab plane. Hence the effective area for the supercurrents should be reduced by the factor

$$0.5\xi_{ab}t/\tan(0.5\theta)$$

for a film of thickness t, which indicates that the critical currents crossing a bicrystal boundary should be inversely proportional to $\tan(0.5\theta)$. The predicted dependence is compared directly with experimental data reported by Dinos *et al.*[1] in Fig. 6. Despite our crude model, the agreement is surprisingly good.

In summary, the surface of an artificial bicrystal boundary has been imaged directly using STM with atomic resolution. Observations of the bicrystal boundary structure by STM and HRTEM are consistent with each other. Upon high-temperature annealing, faceting and etch of both crystals parts occurs, resulting in a zigzagged and grooved grain boundary. These observations of faceting and etching at a bicrystal boundary may open the way for designing and controlling the structure of the grain boundary on an atomic scale. For example, a small-angle bicrystal could be used to generate a boundary with a very sharp and narrow grooving structure. The atomic scale structures of a bicrystal boundary surface observed here with the STM provide hints for a microscopic understanding of the weak link behavior of Josephson junctions based on bicrystal boundaries.

We would like to thank Manual Cardona for a critical reading of the manuscript, and Wolfgang Stiepany for skillful technical assistance. This work was supported by the German BMBF (formerly BMFT) under Contract No. 13N5840.

[1] D. Dinos, P. Chaudhari, J. Mannhart, and F. K. LeGoues, Phys. Rev. Lett. **61**, 219 (1988).
[2] R. Gross, P. Chaudhari, M. Kawasaki, M. B. Betchen, and A. Gupta, Appl. Phys. Lett. **57**, 727 (1990).
[3] Z. Ivanov, P. Å. Nilsson, D. Winkler, J. A. Alarco, and T. Claeson, Appl. Phys. Lett. **59**, 3030 (1991).
[4] Y. Q. Shen, Z. J. Sun, R. Kromann, T. Holst, P. Vase, and T. Freloft, Appl. Phys. Lett. **67**, 2081 (1995).
[5] P. G. Quincey, Appl. Phys. Lett. **64**, 517 (1994).
[6] J. Mannhart, H. Hilgenkamp, B. Mayer, Ch. Gerber, J. R. Kirtley, K. A. Moler, and M. Sigrist, Phys. Rev. Lett. **77**, 2782 (1996).
[7] J. R. Kirtley, C. C. Tsuei, Martin Rupp, J. Z. Sun, Lock See Yu-Jahnes, A. Gupta, and M. B. Ketchen, Phys. Rev. Lett. **76**, 1336 (1996).
[8] C. C. Tsuei *et al.*, Phys. Rev. Lett. **73**, 593 (1994).
[9] J. H. Miller *et al.*, Phys. Rev. Lett. **74**, 2347 (1995).
[10] V. Ravikumar and Vinayak P. Dravid, Ultramicroscopy **52**, 557 (1993).
[11] A. Kazimirov, J. Zegenhagen, I. Denk, J. Maier, D.-M. Smilgies, and R. Feidenhans'l, Surf. Sci. **352-354**, 875 (1996).
[12] C. Traeholt, J. G. Wen, H. W. Zandbergen, Y. Shen, and J. W. M. Hilgenkamp, Physica C **230**, 425 (1994).
[13] M. Naito and H. Sato, in *Advanced Materials '94, VI/A: Superconductors, Surfaces and Superlattices*, edited by H. Sakaki *et al.* [Trans. Mater. Res. Soc. Jpn. **19A**, 533 (1994)].
[14] M. Naito and H. Sato, Physica C **229**, 1 (1994).
[15] Q. D. Jiang and J. Zegenhagen, Surf. Sci. **367**, L42 (1996).
[16] X. Pan, H. Gu, S. Stemmer, and M. Rühle, Mater. Sci. Forum **207-209**, 421 (1996).
[17] T. Haage, H.-U. Habermeier, and J. Zegenhagen, Surf. Sci. **370**, L158 (1997).
[18] W. D. Kingery, H. K. Bowen, and D. R. Uhlmannin, in *Introduction to Ceramics*, 2nd Ed. (Wiley, New York, 1976), p. 212.